Controlled Alloying of the Core–Shell Interface in CdSe/CdS Quantum Dots for Suppression of Auger Recombination

Wan Ki Bae,[‡] Lazaro A. Padilha,[‡] Young-Shin Park, Hunter McDaniel, Istvan Robel, Jeffrey M. Pietryga,[*] and Victor I. Klimov[*]

Center for Advanced Solar Photophysics, Los Alamos National Laboratory, Los Alamos, New Mexico 87545, United States. [‡]W.K.B. and L.A.P. contributed equally to this work.

ABSTRACT The influence of a $CdSe_xS_{1-x}$ interfacial alloyed layer on the photophysical properties of core/shell CdSe/CdS nanocrystal quantum dots (QDs) is investigated by comparing reference QDs with a sharp core/shell interface to alloyed structures with an intermediate $CdSe_xS_{1-x}$ layer at the core/shell interface. To fully realize the structural contrast, we have developed two novel synthetic approaches: a method for fast CdS-shell growth, which results in an abrupt core/shell boundary (no intentional or unintentional alloying), and a method for depositing a $CdSe_xS_{1-x}$ alloy layer of controlled composition onto the CdSe core prior to the growth of the CdS shell. Both types of QDs possess similar size-dependent single-exciton properties (photoluminescence energy, quantum yield, and decay lifetime). However the alloyed QDs show a significantly longer biexciton lifetime and up to a 3-fold increase in the biexciton emission efficiency compared to the reference samples. These results provide direct evidence that the structure of the QD interface has a significant effect on the rate of nonradiative Auger recombination, which dominates biexciton decay. We also observe that the energy gradient at the core–shell interface introduced by the alloyed layer accelerates hole trapping from the shell to the core states, which results in suppression of shell emission. This comparative study offers practical guidelines for controlling multicarrier Auger recombination without a significant effect on either spectral or dynamical properties of single excitons. The proposed strategy should be applicable to QDs of a variety of compositions (including, *e.g.*, infrared-emitting QDs) and can benefit numerous applications from light emitting diodes and lasers to photodetectors and photovoltaics.

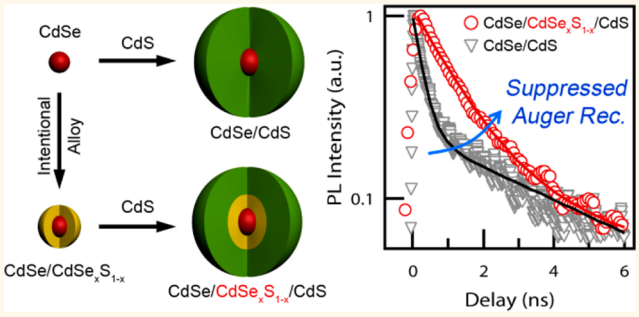

KEYWORDS: nanocrystal · quantum dot · core/shell · alloyed core/shell interface · CdSe/CdS · $CdSe/CdSe_xS_{1-x}/CdS$ · Auger recombination

Nanocrystal quantum dots (QDs) are promising materials for optoelectronic applications due to their exceptional optical properties, such as high photoluminescence (PL) quantum yield (QY), narrow emission line width, size-tunable band gap over a wide range of energies, and solution processability.[1] More recent synthetic efforts have extended beyond traditional size/shape control and often involve engineering of the internal structure of the QD in order to manipulate, for example, single-exciton dynamics and carrier–carrier interaction energies. A notable example is the control over single-exciton radiative recombination in type-II and *quasi*-type-II heterostructured QDs.[2−6] Type-II heterostructuring has been also applied to realize "giant" exciton–exciton repulsion used in the demonstration of the single-exciton optical gain regime.[7,8]

In contrast to substantial progress in understanding and manipulating single-exciton dynamics, practical control over multiexciton dynamics in QDs has been much more difficult to achieve, despite its inherent importance for utilization of QDs in devices. Suppression of nonradiative Auger recombination (AR), which otherwise is highly efficient in standard nanocrystals of all compositions and shapes,[9−11] is of particular interest for the realization of QD devices such as

* Address correspondence to pietryga@lanl.gov, klimov@lanl.gov.

Received for review January 18, 2013 and accepted March 22, 2013.

Published online March 23, 2013
10.1021/nn4002825

high-brightness light-emitting diodes (LEDs), low-threshold lasers and third-generation photovoltaics enabled by carrier multiplication.[10,12]

Recently, reduced AR rates and/or reduced PL "blinking" have been observed in CdSe/CdTe,[13] CdZnSe/ZnSe,[14] and in high-quality thin-[15] or thick-shell CdSe/CdS heterostructured QDs.[16−19] Although a promising first step, attempts to achieve more complete and consistent AR suppression have been frustrated by uncertainty regarding the mechanism responsible for the effect. Some spectroscopic findings[14,16] and theoretical studies[20,21] have suggested that the sharpness of the electronic confinement potential defined by structure of the core/shell interface may have a crucial effect on the AR rate. However, experimental studies of the role of the interfacial potential in AR are greatly complicated by the lack of reliable chemical means for controlling the composition of the core/shell interface because of commonly observed processes such as unintentional alloying,[16] which can result from the application of prolonged reaction times, or especially high reaction temperatures.

Here, we present for the first time a comparative study of the influence of the structure of the core/shell interfacial layer on the electronic and photophysical properties of QDs, and specifically, on AR time constants. This study has been enabled by new synthetic methods that allow us to fabricate thick-shell CdSe/CdS QDs with either a sharp core/shell interface or an interface smoothened by an intermediate $CdSe_xS_{1-x}$ alloy layer of controlled thickness and composition. Detailed spectroscopic analysis reveals that a $CdSe_xS_{1-x}$ alloy interface layer has very little effect on the behavior of single excitons in these heterostructures (*e.g.*, PL decay lifetime or QY), but plays a significant role in the suppression of AR as indicated by the dramatic effect on biexciton dynamics. A significant suppression of AR observed in the CdSe/$CdSe_xS_{1-x}$/CdS QDs can be attributed to the decreased steepness of the confinement potential experienced by core-localized holes, which reduces the likelihood of its intraband re-excitation *via* AR.[20] This study offers a practical approach for significant suppression of AR in nanocrystal QDs beneficial to a wide range of optical and optoelectronic applications of these nanostructures.

RESULTS AND DISCUSSION

Although the optical properties of CdSe/CdS QDs have been extensively studied experimentally and theoretically,[4,16,17,22−28] there is as-of-yet no direct comparison between equivalent QDs with and without appreciable alloying at the core/shell interface. Previously, thick-shell CdSe/CdS QDs have been produced by a successive ionic layer adsorption and reaction (SILAR) method, which requires consecutive multiple precursor injection steps along with lengthy precursor reaction times for each step.[27] The prolonged exposure of CdSe/CdS QDs to elevated temperatures causes interfacial alloying as a result of uncontrolled interdiffusion of Se and S atoms at the interface, which has been speculated to be the key factor for suppression of AR.[16]

As the first step toward elucidating the effect of the core/shell interface on photophysical properties of CdSe/CdS QDs, we have developed a new method for a fast growth of the CdS shell which allows us to realize QDs with a sharp interfacial profile (hereafter referred to as C/S QDs; Figure 1). The CdS shell growth is performed on top of a zinc blende (ZB) CdSe core using a single continuous injection of Cd and S precursors, rather than multiple alternating Cd and S precursor injections applied in the SILAR method. The result is a dramatic reduction in the total reaction time; for example, it takes 45 h using the SILAR method to grow a 15 ML CdS shell,[4,25] whereas the same thickness is achieved in only 5 h *via* the fast CdS shell growth introduced in this study. The synthesized C/S QDs show a significant red shift of the PL and the 1S band-edge absorption peaks (Figure 1a) and a gradual increase in the PL single-exciton lifetime (Figure 1b,c) with increasing shell thickness. Simultaneously, the PL QY first dramatically increases compared to core-only QDs and then gradually falls off (Figure 1d).

The observed changes in spectroscopic properties of the C/S structures are similar to the trends seen previously in CdSe/CdS QDs fabricated by SILAR.[4,5,24] This suggests that the C/S QDs prepared by the fast shell growth method possess a similar *quasi*-type II electronic structure, in which the electron is largely delocalized over the entire QD volume, while the hole is strongly confined within the CdSe core.[4,16,17,24] Both the increase in lifetime and decrease in QY are, then, consistent with the resulting reduction in electron−hole wave function overlap. The C/S QDs maintain a roughly spherical shape as long as the total radius (R) is smaller than 4−5 nm (Figure 1e−h; the CdSe core radius is r = 1.5 nm); samples in Figure 1 are labeled using notation r(nm)/H(nm), where H is the shell thickness. For larger sizes, QDs become more faceted due to the influence of the underlying ZB crystal structure (Supporting Information). The size distribution broadens slightly during growth, as evidenced by the width of the PL peak, which grows from 27 to 36 nm (Figure 1a, inset). Importantly, we observe no evidence of small CdS QDs throughout the entire reaction, indicating that injected Cd and S precursors do not produce a significant homogeneous nucleation event.

For comparison to the reference C/S QDs, we synthesized "interface-alloyed" samples in which a $CdSe_xS_{1-x}$ layer of controlled thickness (L; generally 1.5 nm for the purposes of the present study) is grown onto the CdSe core (hereafter referred to as C/A QDs) or between the CdSe core and the CdS shell (C/A/S QDs). For the growth of the alloyed layer, we continuously inject a

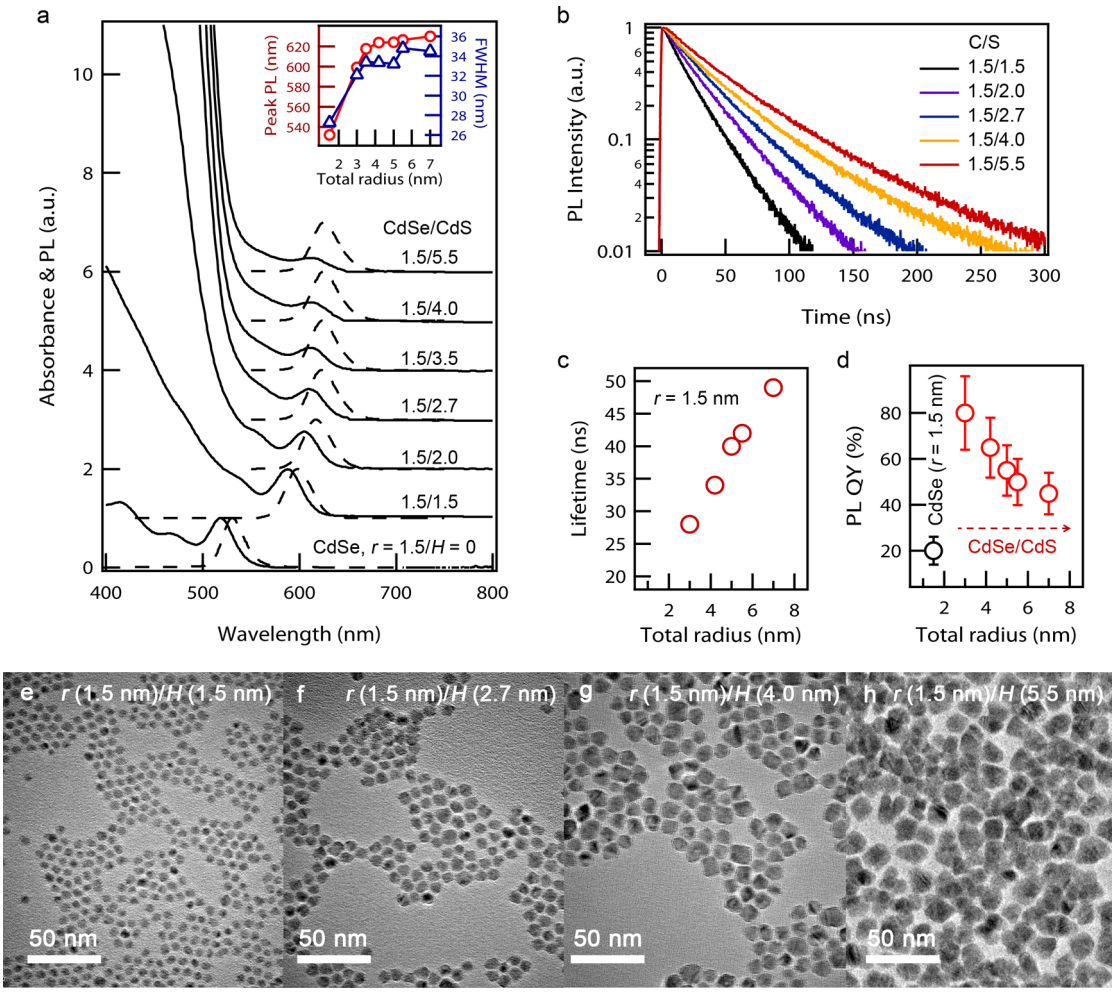

Figure 1. Photophysical properties of fast-grown core/shell (C/S) CdSe/CdS QDs with the same core size (r = 1.5 nm) and different shell thicknesses ($0 \leq H \leq 5.5$ nm). (a) Optical absorption and PL spectra; sample labels show r(nm)/H(nm). Inset: peak PL wavelength (red circles) and full width at half maximum (FWHM) (blue triangles) as a function of total radius ($R = r + H$). (b) Single exciton PL decay dynamics, (c) PL lifetimes, (d) PL QYs, and (e–h) transmission electron microscopy (TEM) images of C/S QDs of varied sizes.

mixture of Se and S precursors (1:1 in molar ratio) at elevated temperature into a reaction flask containing CdSe cores and excess Cd precursor (Figure 2a). The $CdSe_xS_{1-x}$ alloy shell growth is consistent and highly uniform throughout the tested range of thicknesses (up to 1.5 nm). The C/A particles remain mostly spherical (Figure 2b) and retain excellent size dispersity, as evidenced by the distinct excitonic features in their absorption spectra and a narrow PL bandwidth (full width at half-maximum, fwhm, is ~25 nm; Figure 2c,d). The C/A samples exhibit a slightly larger red shift in absorption and PL spectra (up to ~100 nm) compared to C/S QDs (~70 nm; see Supporting Information) of the same total radius, which is an expected consequence of increased carrier delocalization into the shell due to lower conduction/valence band offsets. A side-by-side analysis of QD sizes (characterized by transmission electron microscopy, TEM) and elemental composition (characterized by energy-dispersive X-ray, EDX, spectroscopy) of aliquots taken during the alloy layer growth reveals that it has a fairly constant composition along the radial direction, which is close to the ratio of injected amounts of Se and S (Se:S = 1:1) with only a slight composition gradient (Se content varies from 0.56 to 0.49 from thin to thick shells; see Figure 2e and Supporting Information).

Overgrowing the C/A CdSe/$CdSe_xS_{1-x}$ QDs with a CdS shell by the fast growth method allows us to fabricate C/A/S samples with a smoothened core/shell interface, and then compare their photophysical properties with those of reference C/S QDs with a sharp interfacial profile (Figure 3). As the CdS shell thickness is increased, both types of QDs show a similar gradual red shift of the 1S absorption feature and the PL band as well as an increase in the PL lifetime (see Figure 3 and Supporting Information), again confirming that both structures possess a similar quasi-type II electronic structure.[4,16,17,24,25] Interestingly, the 3 nm radius CdSe/$CdSe_xS_{1-x}$ C/A QDs exhibit a lower PL QY than the same-size CdSe/CdS C/S QDs, which we attribute to a reduced valence-band offset in the former case, which results in more frequent interactions of core-localized holes with

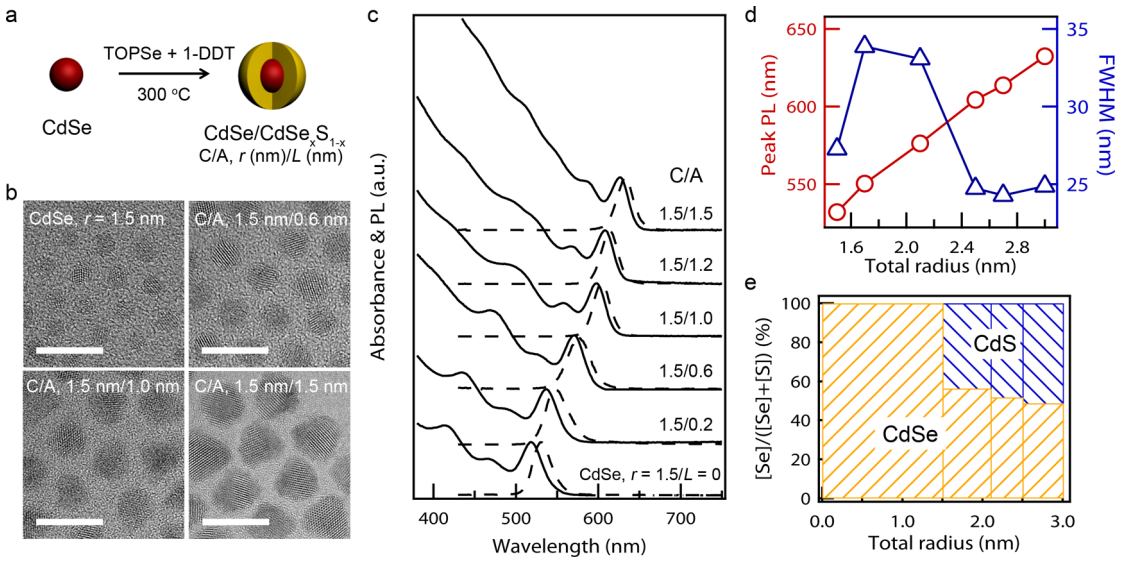

Figure 2. Synthesis of core/alloy (C/A) CdSe/CdSe$_x$S$_{1-x}$ QDs and their structural and optical properties. (a) Synthetic scheme illustrating fabrication of the CdSe$_x$S$_{1-x}$ alloy layer on top of CdSe cores. TEM images (b; scale bar is 10 nm), absorption and PL spectra (c), and peak PL wavelength along with PL FWHM (d) for C/A QDs with the same core radius (r = 1.5 nm) and various thicknesses of the alloy layer (L); sample labels show r(nm)/L(nm). (e) Elemental composition across the CdSe$_x$S$_{1-x}$ alloy layer determined by correlating the average QD size from TEM and the results of elemental analysis using EDX spectroscopy.

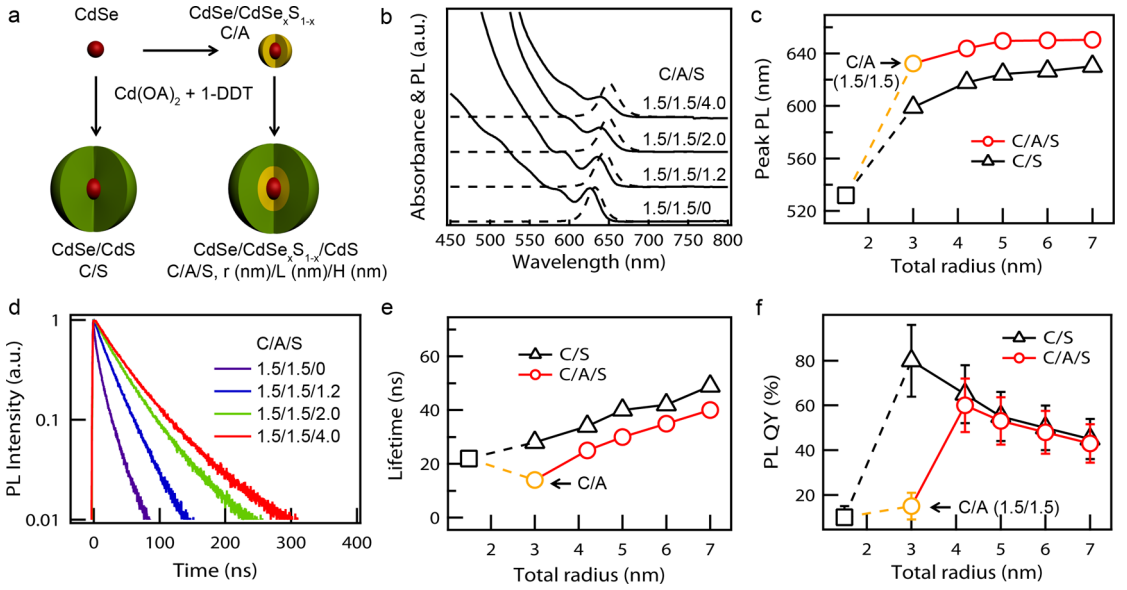

Figure 3. Synthesis and spectroscopic characterization of reference core/shell (C/S) CdSe (r = 1.5 nm)/CdS QDs with an abrupt interface and core/alloy/shell (C/A/S) CdSe (r = 1.5 nm)/CdSe$_x$S$_{1-x}$ (1.5 nm)/CdS QDs with an alloyed interface. (a) Schematic illustration of synthesis for both types of QDs. (b) Optical absorption and PL spectra of C/A/S QDs as a function of shell thickness (H); sample labels show r(nm)/L(nm)/H(nm). Peak PL wavelength (c), single-exciton PL decay dynamics (d), PL lifetimes (e), and QYs (f) for reference C/S (black symbols) *vs* alloyed C/A/S (colored symbols) QDs.

surface traps. Accordingly, the PL QY of the C/A/S QDs increases with increasing the CdS shell thickness, and eventually approaches the same values as those for C/S QDs of a similar size. This observation offers further indication that the CdSe$_x$S$_{1-x}$ alloy layer does indeed provide an intermediate potential step between the CdSe core and the CdS shell with very little influence on intrinsic single exciton dynamics.

To determine the influence of the alloy layer on multiexciton decay, we compare spectrally resolved PL dynamics of C/S reference QDs and C/A/S alloyed QDs of the same overall size (R = 7 nm) as a function of excitation intensity (Figure 4). Both types of samples show strong CdSe core emission (625−650 nm) at all pump intensities, indicating that the CdSe core is the primary emitting center for single and multiexciton emission in both types of QDs. Interestingly, a new PL band at a shorter wavelength (~518 nm; corresponds to the expected band gap of the CdS shell) emerges in the reference C/S sample at intensities above 5 μJ/cm^2

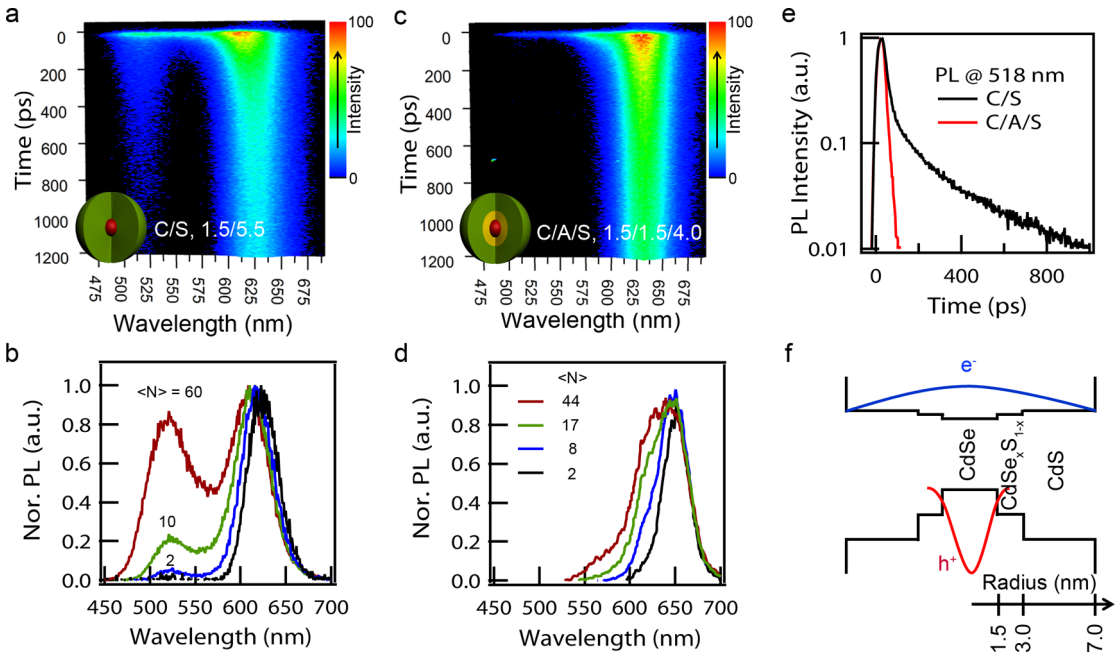

Figure 4. Pump-intensity-dependent transient photoluminescence of C/S and C/A/S QDs with the same core radius (r = 1.5 nm) and the same total radius (R = 7 nm); the alloy layer thickness (L) in the C/A/S structures is 1.5 nm (streak camera measurements using pulsed excitation at 3.1 eV). Spectrally resolved PL traces with photoexcitation at 3.1 eV with average number of excitons per dot ($\langle N \rangle$) of 16 for the C/S (a) and 22 for the C/A/S (c) QDs. Normalized PL spectra obtained by binning the first 0-to-100 ps of streak-camera data for different pump fluences (indicated in the figure) for C/S (b) and (d) C/A/S QDs. (e) PL decay dynamics measured at 518 nm; $\langle N \rangle$ = 81 for the C/S and 110 for the C/A/S QDs. (f) Approximate energy band diagram of C/A/S QDs along with spatial distributions of electron and hole wave functions.

(Figure 4a,b), while this feature is *not* present in the spectrum of the C/A/S sample even at intensities as high as 150 μJ/cm^2 (Figure 4c,d). This observation can be rationalized if we examine decay dynamics of CdS shell emission measured for these samples (Figure 4e). The decay observed in the alloyed QDs is significantly shorter compared to that in the reference sample, suggesting that the intermediate alloy layer creates an energy gradient which facilitates hole migration from the CdS shell to the CdSe core (Figure 4f); as a result of a very short hole residence time within the shell regime, the shell emission is not well pronounced in the C/A/S QDs. In CdSe/CdS QDs without intentional alloying and an exceptionally thick shell (so-called *dot-in-bulk* structures), the interfacial layer can even present a potential barrier for holes, which leads to the effective hole blockade and very efficient dual (core and shell) emission even with low-intensity steady state excitation.[29]

Although both types of the QDs show similar size-dependent trends in single exciton dynamics, clear differences are observed in the multicarrier dynamics (Figure 5a,b). As excitation intensity increases in both cases we observe the emergence of two distinct fast components in the PL traces. We attribute the initial faster component to neutral and charged biexcitons (time constants τ_{xx} and τ_{xx^*}, respectively), while the slower component to charged excitons or "trions" (τ_{x^*}, Figure 5c). To confirm this assignment, we compare the PL decay of the alloyed sample measured under static and stirred conditions (Figure 5d). It is well established that the effect of charging on PL decay dynamics can be diminished by vigorously stirring a QD sample solution during the measurements, as this prevents the fairly slow buildup of a population of charged nanocrystals within the excitation volume.[30,31] Indeed, the amplitude of the intermediate τ_{x^*} component noticeably increases under static conditions (Figure 5d). Simultaneously, the PL peak amplitude also grows (inset of Figure 5d) due to the increased contribution from charged biexcitons that are characterized by a higher emission rate compared to neutral biexcitons.[32] Importantly, the apparent result of this comparison is that the lifetimes of biexcitons and charged species (trions and charged biexcitons) are appreciably longer in the alloyed QDs (by a factor of up to ~3; see table in Figure 5c), implying that AR, which is the dominant channel of their decay,[32] has been partially suppressed as a result of incorporation of the intermediate alloy layer at the core/shell interface.

To compare relative contributions of AR to carrier population decay across different types of QDs, it is informative to consider the effective biexciton PL QY (QY_{xx}). To do so, we use the measurements on stirred samples, in which the effect of photocharging is minimized and the initial fast component in high-pump intensity traces is primarily due to neutral biexcitons. Assuming that the dynamics shown in Figure 1b are dominated by single-exciton radiative decay[5] (see section Characterization in Methods), and further using free-carrier scaling of radiative decay rates (previously observed for many types of the QDs, see, *e.g.*, refs 18 and 32), we obtain

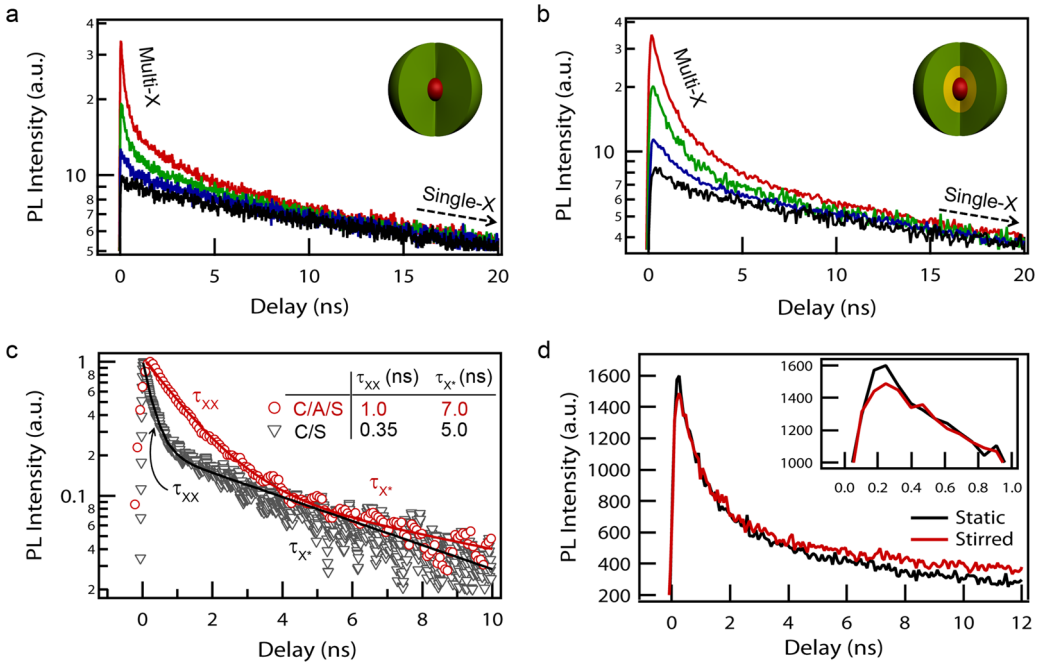

Figure 5. Pump-intensity-dependent PL decay dynamics of C/S CdSe/CdS QDs (a) and C/A/S CdSe/CdSe$_x$S$_{1-x}$/CdS QDs (b) with the same core radius (r = 1.5 nm) and the same total radius (R = 7 nm); for the C/A/S sample L = 1.5 nm. PL decay traces measured with excitation at 3.1 eV with varied average number of excitons per dot ($\langle N \rangle$, 0.02−1.4 for C/S QDs and 0.1−14 for C/A/S QDs) normalized to match long-time single-exciton signals. (c) Early time multiexciton decay dynamics in C/S (gray triangles) and C/A/S (red circles) samples and corresponding fits. (d) Multiexciton decay traces of the C/A/S sample ($\langle N \rangle$ = 7) under static and stirred conditions (inset: expanded PL decay trace for the first 1 ns).

TABLE 1. Photophysical Properties of a Series of C/S and C/A/S QD Samples[a]

	type	core radius (nm)	total radius (nm)	PL peak (nm)	fwhm (nm)	PL QY (%)	τ_x (ns)	τ_{xx} (ns)	τ_{x^*} (ns)	QY$_{xx}$ (%)
1.	C/S	1.5	7.0	630	34.5 (±0.2)	45	49	0.35	5.0	2.9
2.	C/S	2.0	7.0	654	31.5 (±0.2)	40	57	0.75	5.9	5.3
3.	C/A/S	1.5	4.2	644	27.4 (±0.1)	60	25	0.43	5.8	6.9
4.	C/A/S	1.5	7.0	650	28.2 (±0.2)	43	40	1.0	7.0	10.0
5.	C/A/S	1.5	8.0	656	33.7 (±0.1)	30	58	1.6	11.5	11.0

[a] All C/A/S QDs have the same alloy layer thickness (1.5 nm) and Se and S compositional profiles similar to that shown in Figure 2e. Detailed optical properties of C/S CdSe (r = 2.0 nm)/CdS QDs with different CdS shell thicknesses are displayed in Supporting Information. The PL QY was calculated by comparing the integrated PL intensity of QDs to that of a reference dye (LD 690 perchlorate) with the same optical density (0.05) at the excitation wavelength (540 nm). We calculate QY$_{xx}$ from $4\tau_{xx}/\tau_x$ based on the assumption that the radiative biexciton lifetime is 4 times shorter than the single exciton lifetime.

that the radiative lifetime of biexcitons ($\tau_{xx,r}$) can be related to the measured single exciton lifetime (τ_x) by $\tau_{xx,r} = \tau_x/4$. This further yields the following expression: QY$_{xx} = 4\tau_{xx}/\tau_x$.

In Table 1, we summarize our measurements of τ_x and τ_{xx} as well as single-exciton and biexciton PL efficiencies. To better understand the data one should realize that in thick-shell CdSe/CdS QDs, characterized by strongly asymmetric confinement of electrons and hole, AR is dominated by a fast *positive-trion* pathway,[33] in which the electron−hole recombination energy is transferred to a strongly confined hole. The dominance of this specific AR channel leads also to Auger ionization events[34] dominated by hole ejection from the QD, which leaves behinds an uncompensated electron.[33] As a result, photoexcitation produces primarily *negative trions* that decay *via* the slower Auger pathway involving re-excitation of a delocalized electron. Because of this asymmetry, the Auger lifetime of a biexciton and a negative trion in these hetero-QDs *cannot* be related by the universally accepted statistical scaling observed in monocomponent and thin-shell QDs,[35] that is, τ_{x^*}/τ_{xx} is not necessarily 4. Instead, our measurements for thick-shell CdSe/CdS QDs indicate that the τ_{x^*}/τ_{xx} ratio is from ~7 to ~14. In addition to the breakdown of statistical scaling, deviation of the τ_{x^*}/τ_{xx} ratio from 4 is due to the fact that Auger decay in thick-shell QDs is suppressed compared to standard QDs,[16−19] and therefore, the measured lifetimes are contributed to not only by AR (as is the case in standard QDs) but also radiative recombination characterized by comparable time scales (especially for negative trions).[33]

For reference C/S QDs (lines 1 and 2 of Table 1), we observe that the increase in core size for a fixed total radius affects primarily the lifetime of the biexciton but not the

trion. This is the expected behavior for the negative trion, as the change in the core radius changes primarily the confinement of the hole without modifying the electron confinement (because of its delocalization into the shell). As a result, it does not significantly affect the negative-trion recombination rate (only through its weaker radiative component) but *does* modify the rate of the positive-trion Auger channel, and hence the biexciton lifetime.

Lines 3−5 of Table 1 document the effect of interfacial alloying on Auger lifetimes. Perhaps, the most illustrative comparison is between similarly sized C/S reference and C/A/S alloyed samples in lines 1 and 4, respectively. These two samples have the same core size (r = 1.5 nm) and the same overall dimensions (R = 7 nm) but the shell of the alloyed sample includes a thin 1.5 nm $CdSe_xS_{1-x}$ layer adjacent to the core. These two samples have nearly identical single-exciton properties (see data for R = 7 nm in Figure 3c,e,f) indicating only a minor effect of the intermediate alloy layer on localization of both electrons and holes. At the same time, interfacial alloying has a dramatic effect on the biexciton lifetime (almost 3-fold lengthening), indicating significant suppression of the Auger channel involving re-excitation of the hole. This result is consistent with the theory of Cragg and Efros[20] according to which the overlap of the initial and the final states of the Auger carrier re-excited in the recombination event controls the rate of this process, which means that in the case of heterostructured QDs, the smoother the potential, the slower the rate. Since in our samples, the core−shell interface is "seen" primarily by a core-localized hole, its smoothening should mostly affect the positive-trion Auger pathway, in agreement with our experimental observations. A weak but clearly discernible influence of potential smoothening on the trion lifetimes suggests that it also affects the negative-trion pathway, but to a lesser degree as the electron wave function is delocalized across the entire QD volume, and therefore is less sensitive to the properties of the core−shell interface than the hole wave function.

The effect of interfacial alloying is also evident in the case of the two other C/A/S samples shown in lines 3 and 5 of Table 1. On the basis of volume scaling, the C/A/S QDs with R = 4.2 nm (line 3) should show shortening of the biexciton lifetime compared to the reference samples in line 1 (R = 7 nm); instead, the biexciton lifetime in the C/A/S sample is longer, confirming again the importance of the structure of the core/shell interface. The combined effect of volume scaling and potential smoothing results in the longest τ_{xx} constant measured for the largest C/A/S QDs shown in line 5. As expected, these nanocrystals also show the largest QY_{xx}. In fact, all three C/A/S samples, independent of their exact dimensions and even including the smallest one, exhibit consistently higher biexciton emission efficiencies compared to the reference C/S samples.

We would like to point out that the improvement in QY_{xx} observed in the present study for intentionally alloyed C/A/S samples is still lower than the record values measured in single-dot studies for some of the QDs in samples grown by a traditional SILAR method.[18] Indeed for reason of diffusion kinetics SILAR can produce a thicker and a more compositionally graded layer (at least in a subset of the QDs) than for a single potential step used in the present study. It is worth noting, however, that the distribution of biexciton PL QYs inferred from single-dot measurements of SILAR samples[18] is quite wide, which is also consistent with the formation of a range of gradient structures, some more effective, some less, within the ensemble. A clear next step, therefore, is to vary the growth conditions of C/A/S QDs, such as to intentionally create a smoother compositional gradient (i.e., more potential steps) within the alloy layer across the entire QD ensemble, which according to recent predictions[20] can result in overall reduction of AR rates by 1−3 orders of magnitude, depending on the exact shape of the confinement potential.

CONCLUSIONS

We have studied the influence of the interfacial $CdSe_xS_{1-x}$ alloy layer on photophysical properties of CdSe/CdS core/shell QDs. For a truly distinct structural contrast, CdSe/CdS QDs with a sharp core/shell interface have been synthesized by a new fast CdS shell growth method, which allowed us to fabricate QDs with and without a $CdSe_xS_{1-x}$ alloy layer between a CdSe core and a CdS shell. Detailed spectroscopic studies have revealed that the presence of the interfacial alloy layer has little effect on single-exciton dynamics but has a significant influence on multiexciton decay, and particularly leads to appreciable AR suppression. We attribute this effect primarily to a reduction in the steepness of the hole confinement potential at the core−shell interface due to the intervening $CdSe_xS_{1-x}$ layer acting as an intermediate potential step. This comparative study not only clearly demonstrates the influence of the interface structure on the photophysical properties of heterostructured QDs but also suggests a clear means for further enhancing control over multiexciton dynamics through *interface engineering*, which can complement traditional means such as size/shape control and type-I and type-II heterostructuring.

METHODS

General Considerations. Cadmium oxide (CdO, 99.998%), Se (200 mesh, 99.999%), 1-dodecanethiol (DDT, 98%), oleic acid (OA, 99%), 1-octadecene (ODE, 90%), tri-*n*-octylphosphine (TOP, 97%) and tri-*n*-octylamine (TOA, 95%) were purchased from Alfa Aesar. Organic solvents were purchased from Fisher Chemical.

LD690 perchlorate (reference dye for PL QY measurement) was purchased from Exciton. All chemicals were used without further purification. All syntheses were performed under inert atmosphere using standard Schlenk-line and glovebox techniques. Cadmium oleate [0.5 M, $Cd(OA)_2$] complex was prepared by heating 5 mmol of CdO with 5 mL of OA at 300 °C for 1 h, and then diluting with TOA to a total volume of 10 mL. Trioctylphosphine selenium [1 M, TOPSe] complex was prepared by stirring 1 mmol of Se with 1 mL of TOP at room temperature overnight.

Synthesis of CdSe and CdSe/$CdSe_xS_{1-x}$ QDs. CdSe QDs with radius of 1.5 nm were synthesized by a previously reported method.[36] Prepared CdSe QDs were repeatedly purified by precipitating with ethanol and redispersing in toluene. Final products were dispersed in ODE at a concentration of 0.015 mM. For the synthesis of CdSe/$CdSe_xS_{1-x}$ QDs, 2 mL of CdSe core solution were added to a flask containing 8 mL of TOA and 0.6 mL of 0.5 M $Cd(OA)_2$ at 300 °C. A mixture of TOPSe (0.15 mL of 1 M solution) and DDT (0.15 mmol) diluted with TOA (total volume: 1 mL) was slowly injected into the reaction flask over 30 min. Aliquots were taken during the reaction for characterization.

Fast CdS Shell Growth on CdSe or CdSe/$CdSe_xS_{1-x}$ QDs. Fabrication of an CdS shell was carried out *via* continuous injection of $Cd(OA)_2$ (0.5 M) and DDT (0.5 M, diluted with TOA) at a rate of 2 mL/h into the reaction vessel containing either CdSe or CdSe/$CdSe_xS_{1-x}$ QDs diluted with TOA (total volume: 10 mL). The reaction temperature was maintained at 300 °C throughout the formation of the complete CdS shell. Synthesized QDs were purified repeatedly by a precipitation/dispersion method and dispersed in nonpolar organic solvents for further characterization.

Characterization. The size and composition of QDs were characterized with a TEM (JEOL JEM 2010) equipped with an energy-dispersive X-ray (EDX) spectrometer (Bruker Quantax). EDX spectra were collected at several locations for each TEM sample, and averaged such that each reported composition represents that of several hundred individual QDs. The composition of individual layers, such as during alloy growth, was determined by comparing subsequent aliquots during single growth experiments. Briefly, we compared a given aliquot's size (by TEM) and Se:S (by EDX) to that of the previous aliquot to determine the thickness of the new layer and its effective Se:S ratio (by accounting for the mass-normalized contribution to the measured ratio that comes from the CdSe core and previous alloy layers, if any). The raw Se:S ratios used for these calculations are shown in the Supporting Information (Figure S3).

Optical absorbance was measured with an Agilent 8453 spectrometer; PL spectra and single-exciton decay traces were recorded with a Horiba Fluoromax-4 spectrofluorometer. For spectroscopic measurements, QD samples were loaded into 1 mm path-length spectroscopic-grade cuvettes, and the optical density at 400 nm was adjusted to less than 0.1 to avoid PL reabsorption. When not otherwise noted, the samples were vigorously stirred during measurement to avoid photochemical degradation and photocharging.

Picosecond time-resolved PL measurements shown in Figure 4 were conducted using a Hamamatsu 5860 streak camera with 12 ps time resolution. The samples were excited at 3.1 eV with ~100 fs pulses from a 1 kHz amplified Ti:sapphire laser. In nanosecond PL measurements shown in Figures 1, 3 and 5, the samples were excited at 3.1 eV by ~250 fs pulses from a 250 kHz amplified Ti:sapphire laser and PL dynamics were resolved using time-correlated single-photon counting (TCSPC). These measurements utilized two types of detectors: a microchannel plate photomultiplier tube (PMT; time resolution 150 ps), used for samples with biexciton lifetimes longer than ~300 ps, and a superconducting nanowire single photon detector (SNSPD) with the instrument response time of ~50 ps[37] in studies of samples with shorter biexciton decay times. For microchannel plate detection the collection monochromator was set to the PL peak wavelength while for SNSPD detection the PL was collected through a 610 nm long pass filter, which blocks any contribution of the shell emission. The SNSPD was housed in a closed-loop helium cryocooler and kept at ~3.5 K. The superconducting nanowire of NbN was biased to ~90% of its superconducting critical current (typically ~20 μA). The voltage pulses were amplified and read out with a Picoquant Hydraharp with an 8 ps binning time.

Single exciton radiative lifetimes were determined from monoexponential fits of the low-fluence (no multiexcitons) decay traces acquired with PMT-TCSPC, which yielded time constants of tens of nanoseconds. In these samples, nonradiative losses are primarily due to carrier trapping at surface/interfacial defects, which is characterized by much faster subnanosecond dynamics not resolvable in the PMT-TCSPC measurements. This approach to determining radiative time constants is validated by the fact that the single exciton radiative lifetimes of our thin-shell samples are in good agreement with literature values for well-passivated core-only CdSe QDs.[37]

Conflict of Interest: The authors declare no competing financial interest.

Acknowledgment. This work was performed within the Center for Advanced Solar Photophysics (CASP), an Energy Frontier Research Center funded by the U.S. Department of Energy (DOE), Office of Science, Basic Energy Sciences (BES).

Supporting Information Available: Additional results of spectroscopic and microstructural characterization of reference CdSe/CdS core/shell QDs and alloyed CdSe/$CdSe_xS_{1-x}$ and CdSe/$CdSe_xS_{1-x}$/CdS QDs. This material is available free of charge *via* the Internet at http://pubs.acs.org.

REFERENCES AND NOTES

1. *Nanocrystal Quantum Dots*, 2nd ed.; Klimov, V. I., Ed.; CRC Press: Boca Raton, FL, 2010.
2. Kim, S.; Fisher, B.; Eisler, H.-J.; Bawendi, M. Type-II Quantum Dots: CdTe/CdSe(Core/Shell) and CdSe/ZnTe(Core/Shell) Heterostructures. *J. Am. Chem. Soc.* **2003**, *125*, 11466–11467.
3. Lee, D. C.; Robel, I.; Pietryga, J. M.; Klimov, V. I. Infrared-Active Heterostructured Nanocrystals with Ultralong Carrier Lifetimes. *J. Am. Chem. Soc.* **2010**, *132*, 9960–9962.
4. Chen, Y.; Vela, J.; Htoon, H.; Casson, J. L.; Werder, D. J.; Bussian, D. A.; Klimov, V. I.; Hollingsworth, J. A. "Giant" Multishell CdSe Nanocrystal Quantum Dots with Suppressed Blinking. *J. Am. Chem. Soc.* **2008**, *130*, 5026–5027.
5. Brovelli, S.; Schaller, R. D.; Crooker, S. A.; García-Santamaría, F.; Chen, Y.; Viswanatha, R.; Hollingsworth, J. A.; Htoon, H.; Klimov, V. I. Nano-Engineered Electron–Hole Exchange Interaction Controls Exciton Dynamics in Core–Shell Semiconductor Nanocrystals. *Nat. Commun.* **2011**, *2*, 280.
6. Dabbousi, B. O.; Rodriguez-Viejo, J.; Mikulec, F. V.; Heine, J. R.; Mattoussi, H.; Ober, R.; Jensen, K. F.; Bawendi, M. G. (CdSe)ZnS Core–Shell Quantum Dots: Synthesis and Characterization of a Size Series of Highly Luminescent Nanocrystallites. *J. Phys. Chem. B* **1997**, *101*, 9463–9475.
7. Klimov, V. I.; Ivanov, S. A.; Nanda, J.; Achermann, M.; Bezel, I.; McGuire, J. A.; Piryatinski, A. Single-Exciton Optical Gain in Semiconductor Nanocrystals. *Nature* **2007**, *447*, 441–446.
8. Nanda, J.; Ivanov, S. A.; Achermann, M.; Bezel, I.; Piryatinski, A.; Klimov, V. I. Light Amplification in the Single-Exciton Regime Using Exciton–Exciton Repulsion in Type-II Nanocrystal Quantum Dots. *J. Phys. Chem. C* **2007**, *111*, 15382–15390.
9. Robel, I.; Gresback, R.; Kortshagen, U.; Schaller, R. D.; Klimov, V. I. Universal Size-Dependent Trend in Auger Recombination in Direct-Gap and Indirect-Gap Semiconductor Nanocrystals. *Phys. Rev. Lett.* **2009**, *102*, 177404.
10. Klimov, V. I.; Mikhailovsky, A. A.; McBranch, D. W.; Leatherdale, C. A.; Bawendi, M. G. Quantization of Multiparticle Auger Rates in Semiconductor Quantum Dots. *Science* **2000**, *287*, 1011–1013.
11. Achermann, M.; Bartko, A. P.; Hollingsworth, J. A.; Klimov, V. I. The Effect of Auger Heating on Intraband Carrier Relaxation in Semiconductor Quantum Rods. *Nat. Phys.* **2006**, *2*, 557–561.
12. Semonin, O. E.; Luther, J. M.; Choi, S.; Chen, H.-Y.; Gao, J.; Nozik, A. J.; Beard, M. C. Peak External Photocurrent Quantum Efficiency Exceeding 100% *via* MEG in a Quantum Dot Solar Cell. *Science* **2011**, *334*, 1530–1533.

13. Osovsky, R.; Cheskis, D.; Kloper, V.; Sashchiuk, A.; Kroner, M.; Lifshitz, E. Continuous-Wave Pumping of Multiexciton Bands in the Photoluminescence Spectrum of a Single CdTe-CdSe Core-Shell Colloidal Quantum Dot. *Phys. Rev. Lett.* **2009**, *102*, 197401.
14. Wang, X.; Ren, X.; Kahen, K.; Hahn, M. A.; Rajeswaran, M.; Maccagnano-Zacher, S.; Silcox, J.; Cragg, G. E.; Efros, A. L.; Krauss, T. D. Non-blinking Semiconductor Nanocrystals. *Nature* **2009**, *459*, 686–689.
15. Chen, O.; Zhao, J.; Chauhan, V. P.; Cui, J.; Wong, C.; Harris, D. K.; Wei, H.; Han, H.-S.; Fukumura, D.; Jain, R. K.; Bawendi, M. G. Compact High-Quality CdSe–CdS Core–Shell Nanocrystals with Narrow Emission Linewidths and Suppressed Blinking. *Nat. Mater.* **2013**, 10.1038/nmat3539.
16. García-Santamaría, F.; Brovelli, S.; Viswanatha, R.; Hollingsworth, J. A.; Htoon, H.; Crooker, S. A.; Klimov, V. I. Breakdown of Volume Scaling in Auger Recombination in CdSe/CdS Heteronanocrystals: The Role of the Core–Shell Interface. *Nano Lett.* **2011**, *11*, 687–693.
17. García-Santamaría, F.; Chen, Y.; Vela, J.; Schaller, R. D.; Hollingsworth, J. A.; Klimov, V. I. Suppressed Auger Recombination in "Giant" Nanocrystals Boosts Optical Gain Performance. *Nano Lett.* **2009**, *9*, 3482–3488.
18. Park, Y.-S.; Malko, A. V.; Vela, J.; Chen, Y.; Ghosh, Y.; García-Santamaría, F.; Hollingsworth, J. A.; Klimov, V. I.; Htoon, H. Near-Unity Quantum Yields of Biexciton Emission from CdSe/CdS Nanocrystals Measured Using Single-Particle Spectroscopy. *Phys. Rev. Lett.* **2011**, *106*, 187401.
19. Spinicelli, P.; Buil, S.; Quélin, X.; Mahler, B.; Dubertret, B.; Hermier, J. P. Bright and Grey States in CdSe–CdS Nanocrystals Exhibiting Strongly Reduced Blinking. *Phys. Rev. Lett.* **2009**, *102*, 136801.
20. Cragg, G. E.; Efros, A. L. Suppression of Auger Processes in Confined Structures. *Nano Lett.* **2009**, *10*, 313–317.
21. Climente, J. I.; Movilla, J. L.; Planelles, J. Auger Recombination Suppression in Nanocrystals with Asymmetric Electron–Hole Confinement. *Small* **2012**, *8*, 754–759.
22. Malko, A. V.; Park, Y.-S.; Sampat, S.; Galland, C.; Vela, J.; Chen, Y.; Hollingsworth, J. A.; Klimov, V. I.; Htoon, H. Pump-Intensity- and Shell-Thickness-Dependent Evolution of Photoluminescence Blinking in Individual Core/Shell CdSe/CdS Nanocrystals. *Nano Lett.* **2011**, *11*, 5213–5218.
23. Qin, W.; Guyot-Sionnest, P. Evidence for the Role of Holes in Blinking: Negative and Oxidized CdSe/CdS Dots. *ACS Nano* **2012**, *6*, 9125–9132.
24. Mahler, B.; Spinicelli, P.; Buil, S.; Quelin, X.; Hermier, J.-P.; Dubertret, B. Towards Non-blinking Colloidal Quantum Dots. *Nat. Mater.* **2008**, *7*, 659–664.
25. Ghosh, Y.; Mangum, B. D.; Casson, J. L.; Williams, D. J.; Htoon, H.; Hollingsworth, J. A. New Insights into the Complexities of Shell Growth and the Strong Influence of Particle Volume in Nonblinking "Giant" Core/Shell Nanocrystal Quantum Dots. *J. Am. Chem. Soc.* **2012**, *134*, 9634–9643.
26. Tschirner, N.; Lange, H.; Schliwa, A.; Biermann, A.; Thomsen, C.; Lambert, K.; Gomes, R.; Hens, Z. Interfacial Alloying in CdSe/CdS Heteronanocrystals: A Raman Spectroscopy Analysis. *Chem. Mater.* **2011**, *24*, 311–318.
27. Li, J. J.; Wang, Y. A.; Guo, W.; Keay, J. C.; Mishima, T. D.; Johnson, M. B.; Peng, X. Large-Scale Synthesis of Nearly Monodisperse CdSe/CdS Core/Shell Nanocrystals Using Air-Stable Reagents *via* Successive Ion Layer Adsorption and Reaction. *J. Am. Chem. Soc.* **2003**, *125*, 12567–12575.
28. Zhao, J.; Chen, O.; Strasfeld, D. B.; Bawendi, M. G. Biexciton Quantum Yield Heterogeneities in Single CdSe (CdS) Core (Shell) Nanocrystals and Its Correlation to Exciton Blinking. *Nano Lett.* **2012**, *12*, 4477–4483.
29. Galland, C.; Brovelli, S.; Bae, W. K.; Padilha, L. A.; Meinardi, F.; Klimov, V. I. Dynamic Hole Blockade Yields Two-Color Quantum and Classical Light from Dot-in-Bulk Nanocrystals. *Nano Lett.* **2013**, *13*, 321–328.
30. Padilha, L. A.; Robel, I.; Lee, D. C.; Nagpal, P.; Pietryga, J. M.; Klimov, V. I. Spectral Dependence of Nanocrystal Photoionization Probability: The Role of Hot-Carrier Transfer. *ACS Nano* **2011**, *5*, 5045–5055.
31. McGuire, J. A.; Sykora, M.; Robel, I.; Padilha, L. A.; Joo, J.; Pietryga, J. M.; Klimov, V. I. Spectroscopic Signatures of Photocharging due to Hot-Carrier Transfer in Solutions of Semiconductor Nanocrystals under Low-Intensity Ultraviolet Excitation. *ACS Nano* **2010**, *4*, 6087–6097.
32. McGuire, J. A.; Sykora, M.; Joo, J.; Pietryga, J. M.; Klimov, V. I. Apparent *versus* True Carrier Multiplication Yields in Semiconductor Nanocrystals. *Nano Lett.* **2010**, *10*, 2049–2057.
33. Galland, C.; Ghosh, Y.; Steinbrück, A.; Hollingsworth, J. A.; Htoon, H.; Klimov, V. I. Lifetime Blinking in Nonblinking Nanocrystal Quantum Dots. *Nat. Commun.* **2012**, *3*, 908.
34. Klimov, V. I.; McBranch, D. W. Auger-Process-Induced Charge Separation in Semiconductor Nanocrystals. *Phys. Rev. B* **1997**, *55*, 13173–13179.
35. Klimov, V. I.; McGuire, J. A.; Schaller, R. D.; Rupasov, V. I. Scaling of Multiexciton Lifetimes in Semiconductor Nanocrystals. *Phys. Rev. B* **2008**, *77*, 195324.
36. Yang, Y. A.; Wu, H.; Williams, K. R.; Cao, Y. C. Synthesis of CdSe and CdTe Nanocrystals without Precursor Injection. *Angew. Chem., Int. Ed.* **2005**, *44*, 6712–6715.
37. Sandberg, R. L.; Padilha, L. A.; Qazilbash, M. M.; Bae, W. K.; Schaller, R. D.; Pietryga, J. M.; Stevens, M. J.; Baek, B.; Nam, S. W.; Klimov, V. I. Multiexciton Dynamics in Infrared-Emitting Colloidal Nanostructures Probed by a Superconducting Nanowire Single-Photon Detector. *ACS Nano* **2012**, *6*, 9532–9540.